

# Light vector meson decay constants and the renormalization factor from a tadpole-improved action

Randy Lewis and R. M. Woloshyn

*TRIUMF, 4004 Wesbrook Mall, Vancouver, British Columbia, Canada V6T 2A3*  
(October 1996)

## Abstract

The  $\rho$ ,  $K^*$  and  $\phi$  decay constants and the vector current renormalization factor are studied by using an  $\mathcal{O}(a^2)$  classically-improved, tadpole-improved action. Tree-level calculations are used to show how the classical improvement of the action, involving next-nearest-neighbour timesteps, is transferred to the matrix elements. Simulations are performed on coarse lattices and compared to Wilson results from both coarse and fine lattices. The improved action data are found to resemble Wilson data obtained at 1/3 of the lattice spacing, which is the same degree of improvement that is seen by comparing the mass spectra.

## I. INTRODUCTION

Numerical simulations of QCD can be performed by discretizing Euclidean space-time onto a lattice and working within a finite volume. Physical measurements are then obtained by extrapolating to zero lattice spacing and infinite lattice volume. There are many lattice actions which correspond to continuum QCD in the appropriate limit, and a lot of recent work has focussed on finding actions which reduce the errors due to discrete lattice spacing. The goal is to find actions which provide accurate results on coarsely-spaced lattices and so allow lattice sizes (and therefore computing resources) to be reduced. A progress report on improving actions may be found in Ref. [1].

To demonstrate the value of an improved action, one would like to show that accurate results can be obtained from coarse lattices for a wide variety of quantities. As a first step beyond the mass spectrum, where significant improvements on coarse lattices have already been demonstrated, we consider the decay constants of light vector mesons and the associated vector current renormalization factor. (A preliminary discussion was given in Ref. [2].) An advantage of studying vector currents is the existence of a conserved vector current even at nonzero lattice spacing, which does not get renormalized. Neglecting lattice spacing errors, the matrix element of the conserved current between any initial and final states is identical to the matrix element of the local vector current between those same states, except for the multiplicative “renormalization factor”,  $Z_V$ . In this way,  $Z_V$  can be easily computed. In practice, it has been known for a long time [3] that the determination of  $Z_V$  is quite sensitive to lattice spacing errors, which is another reason that the vector current is valuable for the present work, since it is precisely these errors that should be reduced by an improved action.

The action [4,5] that will be used here is improved at the classical level up to and including  $\mathcal{O}(a^2)$ , and is also improved at the quantum level via the “tadpole factor” of Lepage and Mackenzie [6]. The action has the added feature of being quite simple, since the gauge sector contains only  $1 \times 1$  and  $1 \times 2$  plaquettes, and the fermion sector does not contain the so-called “clover” term and has no need of the associated field transformations.

The mass spectrum of this improved action has been studied numerically in Ref. [7], where it was concluded that data from the original Wilson action [8] at a lattice spacing of  $a \sim 0.1\text{fm}$  can be reproduced with the improved action on lattices with  $a \sim 0.3\text{fm}$ , representing a very substantial saving of computing resources. Other studies of the mass spectrum with the same improved action have produced similar results [9,10].

In this paper it is shown that a comparable degree of improvement is also obtained in the computation of the vector meson decay constants,  $f_\rho$ ,  $f_{K^*}$  and  $f_\phi$ , and the renormalization factor,  $Z_V$ . Sec. II begins with a review of the general methods for calculating vector current matrix elements, and then discusses the particular improved action chosen for this work. Sec. III is used to show explicitly that the quantities to be computed are classically improved. The results of numerical simulations using the improved action are compared to Wilson action results in Sec. IV, and a summary is given in Sec. V.

## II. METHOD OF CALCULATION

The  $\rho$  meson decay constant,  $f_\rho$ , is defined from a continuum matrix element of the local vector current as follows.

$$\langle 0|V_\mu^L|\rho\rangle_{\text{cont}} = \frac{m_\rho^2}{f_\rho}\epsilon_\mu \quad (1)$$

$$V_\mu^L(x) = \bar{\psi}(x)\gamma_\mu\psi(x) \quad (2)$$

A similar definition applies to  $f_{K^*}$  and  $f_\phi$ . Recall that this current is conserved in the continuum.

At nonzero lattice spacing the local current is not conserved, and its matrix element between any initial and final states gets renormalized by a factor  $Z_V$ ,

$$\langle f|V_\mu^L|i\rangle_{\text{cont}} = Z_V(g^2)\langle f|V_\mu^L|i\rangle + \mathcal{O}(a^n) . \quad (3)$$

$g$  is the lattice coupling, and  $\mathcal{O}(a^n)$  represents the contributions from operators of higher mass dimension which are multiplied by powers of the lattice spacing,  $a$ . For the Wilson action these corrections begin at  $\mathcal{O}(a)$ , but for our improved action no  $\mathcal{O}(a, a^2)$  classical terms can appear, and the tadpole factor is expected to approximately minimize terms proportional to the coupling, for example  $\mathcal{O}(g^2a)$  terms.

If all quark flavours have the same mass, then both the improved action and the Wilson action have an exact vector (flavour) symmetry, which implies the existence of a conserved ‘‘Noether’’ current,  $V_\mu^C$ . (Actually, there is not a unique conserved current, and care must be used to choose one that is classically improved to the appropriate order. This will be addressed below.) Because of the nonrenormalization of conserved currents,

$$\langle f|V_\mu^L|i\rangle_{\text{cont}} = \langle f|V_\mu^C|i\rangle + \mathcal{O}(a^n) , \quad (4)$$

which allows  $Z_V$  to be computed from a ratio of matrix elements as follows.

$$Z_V(g^2) = \frac{\langle f|V_\mu^C|i\rangle}{\langle f|V_\mu^L|i\rangle} + \mathcal{O}(a^n) \quad (5)$$

Although  $Z_V$  itself is independent of the initial and final states, the ratio of matrix elements in Eq. (5) is not, so the size of the lattice spacing errors can be estimated by varying  $|i\rangle$  and  $|f\rangle$ . In this work, we will consider four separate choices for the ratio in Eq. (5): a vector current insertion between pseudoscalar meson, vector meson or spin-1/2 baryon states,

$$R_P \equiv \frac{\langle P|V_\mu^C|P\rangle}{\langle P|V_\mu^L|P\rangle} , \quad R_V \equiv \frac{\langle V|V_\mu^C|V\rangle}{\langle V|V_\mu^L|V\rangle} , \quad R_B \equiv \frac{\langle B|V_\mu^C|B\rangle}{\langle B|V_\mu^L|B\rangle} \quad (6)$$

and the decay process,

$$R_D \equiv \frac{\langle 0|V_\mu^C|V\rangle}{\langle 0|V_\mu^L|V\rangle} . \quad (7)$$

In our lattice simulations, states will be created via the following local interpolating fields.

$$\text{pseudoscalar mesons : } \chi^P(x) = \bar{\psi}(x)\gamma_5\psi(x) \quad (8)$$

$$\text{vector mesons : } \chi_\mu^V(x) = \bar{\psi}(x)\gamma_\mu\psi(x) \quad (9)$$

$$\text{spin-}\frac{1}{2}\text{ baryons : } \chi^B(x) = \epsilon_{abc}\psi_a(x) \left[ \psi_b^T(x)C\gamma_5\psi_c(x) \right] \quad (10)$$

( $C$  is the charge conjugation matrix.) The decay constant itself is obtained from simulations of the two-point vector correlator,

$$\sum_{\mathbf{x}} \sum_{\mu=1,3} \langle V_\mu^L(\mathbf{x},t)V_\mu^{L\dagger}(0) \rangle \rightarrow \frac{3m_V^3 e^{-m_V t}}{2(2\kappa)^2 Z_V^2 f_V^2} \quad , \quad \text{for } t \gg 0, \quad (11)$$

which is derived by multiplying Eq. (1) with its hermitian conjugate, converting from continuum to lattice quantities, and performing the appropriate summations. The explicit dependence on  $Z_V$  can be changed by replacing one (or both) of the local currents in Eq. (11) by a conserved current. On a lattice with periodic boundary conditions, another term must be added to the right-hand side of Eq. (11) which decays exponentially from the (periodic) image of the source.

Following the work of Lüscher and Weisz [4], the gauge field term of the improved action involves a sum over  $1 \times 2$  rectangular plaquettes ( $U_{pl}$ ) as well as  $1 \times 1$  elementary plaquettes ( $U_{pl}$ ),

$$S_G(U) = \frac{\beta}{3} \text{ReTr} \left[ \sum_{pl} (1 - U_{pl}) - \frac{1}{20U_0^2} \sum_{rt} (1 - U_{rt}) \right] \quad , \quad (12)$$

where a tadpole factor, defined by

$$U_0 = \langle \frac{1}{3} \text{ReTr} U_{pl} \rangle^{1/4} \quad , \quad (13)$$

has been introduced to absorb the lattice tadpole effects and thereby improve the matching to perturbation theory [6]. The fermion part, which was first introduced more than a decade ago [5], also contains next-nearest-neighbour interactions.

$$\begin{aligned} S_F(\bar{\psi}, \psi; U) = & - \sum_x \bar{\psi}(x)\psi(x) \\ & + \frac{4}{3}\kappa \sum_{x,\mu} \left[ \bar{\psi}(x)(1 - \gamma_\mu)U_\mu(x)\psi(x + \mu) + \bar{\psi}(x + \mu)(1 + \gamma_\mu)U_\mu^\dagger(x)\psi(x) \right] \\ & - \frac{\kappa}{6U_0} \sum_{x,\mu} \left[ \bar{\psi}(x)(2 - \gamma_\mu)U_\mu(x)U_\mu(x + \mu)\psi(x + 2\mu) \right. \\ & \left. + \bar{\psi}(x + 2\mu)(2 + \gamma_\mu)U_\mu^\dagger(x + \mu)U_\mu^\dagger(x)\psi(x) \right] \end{aligned} \quad (14)$$

The presence of next-nearest-neighbour timesteps is a generic consequence of classical improvement beyond  $\mathcal{O}(a)$ , and generates well-known artifacts, e.g. unphysical branches in

the free dispersion relations, discussed for gauge fields in Ref. [13]. The effect is also seen for fermions, as discussed in following sections.

The Noether vector current corresponding to Eq. (14) is

$$\begin{aligned}
V_\mu^C(x) &= \frac{2}{3}\bar{\psi}(x+\mu)(1+\gamma_\mu)U_\mu^\dagger(x)\psi(x) - \frac{2}{3}\bar{\psi}(x)(1-\gamma_\mu)U_\mu(x)\psi(x+\mu) \\
&+ \frac{1}{12U_0}\bar{\psi}(x)(2-\gamma_\mu)U_\mu(x)U_\mu(x+\mu)\psi(x+2\mu) \\
&+ \frac{1}{12U_0}\bar{\psi}(x-\mu)(2-\gamma_\mu)U_\mu(x-\mu)U_\mu(x)\psi(x+\mu) \\
&- \frac{1}{12U_0}\bar{\psi}(x+2\mu)(2+\gamma_\mu)U_\mu^\dagger(x+\mu)U_\mu^\dagger(x)\psi(x) \\
&- \frac{1}{12U_0}\bar{\psi}(x+\mu)(2+\gamma_\mu)U_\mu^\dagger(x)U_\mu^\dagger(x-\mu)\psi(x-\mu) .
\end{aligned} \tag{15}$$

Although this current is conserved, an explicit calculation shows that it is not classically improved to the level of the action because of extra total derivative terms. An improved conserved current could be written as follows [11],

$$V_\mu^{CI}(x) = \frac{12}{13}V_\mu^C(x) + \frac{1}{26}V_\mu^C(x-\mu) + \frac{1}{26}V_\mu^C(x+\mu) , \tag{16}$$

but the offending total derivatives in  $V_\mu^C$  do not contribute to the quantities we wish to compute, as will be shown explicitly in Sec. III, so  $V_\mu^{CI}$  is not required for this work.

### III. CONFIRMING TREE-LEVEL IMPROVEMENT

The matrix elements that are used to obtain  $f_\rho$ ,  $f_{K^*}$ ,  $f_\phi$  and  $Z_V$  can be evaluated analytically at the classical level. We will follow closely the approach and notation of El-Khadra, Kronfeld and Mackenzie [12], paying particular attention to the effects of next-nearest-neighbour interactions, which were not present in the actions of Ref. [12].

#### A. The quark equation of motion

The equation of motion that comes from Eq. (14) can be written in the form

$$\sum_y \left[ \sum_\mu \gamma_\mu \tilde{K}_\mu(x, y) + \tilde{L}(x, y) \right] \psi(y) = 0 \tag{17}$$

where the Fourier transforms of  $\tilde{K}_\mu(x, y)$  and  $\tilde{L}(x, y)$  are

$$iK_\mu(p) = \frac{i}{3}\sin p_\mu a (4 - \cos p_\mu a) \tag{18}$$

$$L(p) = Ma + 4 - \frac{4}{3}\sum_\mu \cos p_\mu a + \frac{1}{3}\sum_\mu \cos 2p_\mu a \tag{19}$$

respectively. The on-shell condition is

$$\sum_{\mu} K_{\mu}^2(p) + L^2(p) = 0 \quad (20)$$

which is a quartic equation in  $\cosh Ea = \cosp_4 a$ . Fig. 1 shows the solutions for 3-momenta in the (1,1,0) direction and  $M = 0$ , compared to the Wilson action result and the continuum  $E = |\mathbf{p}|$  line. Notice that the improved action has artifacts which are restricted to the region of large  $Ea$ , and that the low-energy solution is closer to the continuum for a greater range of  $|\mathbf{p}|a$  than is the Wilson curve.

Also related to our discussion of decay constants is the limit of vanishing 3-momentum,  $\mathbf{p} = 0$ , and Fig. 2 shows the solutions of Eq. (20) versus  $Ma$ . Again, improvement is found with respect to the Wilson action. In this case as well there are next-nearest-neighbour timestep artifacts which, however, remain at high energies for the values of  $Ma$  that we will use in numerical simulations. Note that Eq. (20) is only quadratic in the mass, and becomes the following unique expression for  $Ma$  when  $\mathbf{p} = \mathbf{0}$ .

$$Ma + 1 = \frac{1}{3} [1 + 4\cosh Ea - 2\cosh^2 Ea + (4 - \cosh Ea)\sinh|Ea|] \quad (21)$$

We now seek spinor solutions to the equations of motion,

$$\left[ i \sum_{\mu} \gamma_{\mu} K_{\mu}(p) + L(p) \right] u(\xi, \mathbf{p}) = 0 \quad (22)$$

$$\left[ -i \sum_{\mu} \gamma_{\mu} K_{\mu}(p) + L(p) \right] v(\xi, \mathbf{p}) = 0 \quad (23)$$

where  $\xi = 1, 2$  is the spin index. The equation of motion for  $v$ -spinors has been modified so that from now on  $E$  is always a positive quantity. The solutions are

$$u(\xi, \mathbf{p}) = \left[ \frac{-i\gamma_{\mu} K_{\mu}(p) + L(p)}{\sqrt{2L(p)} [L(p) + \sinh Ea (4 - \cosh Ea) / 3]} \right] u(\xi, \mathbf{0}) \quad (24)$$

$$v(\xi, \mathbf{p}) = \left[ \frac{i\gamma_{\mu} K_{\mu}(p) + L(p)}{\sqrt{2L(p)} [L(p) + \sinh Ea (4 - \cosh Ea) / 3]} \right] v(\xi, \mathbf{0}) \quad (25)$$

where

$$u(1, \mathbf{0}) = \begin{pmatrix} 1 \\ 0 \\ 0 \\ 0 \end{pmatrix}, \quad u(2, \mathbf{0}) = \begin{pmatrix} 0 \\ 1 \\ 0 \\ 0 \end{pmatrix}, \quad v(1, \mathbf{0}) = \begin{pmatrix} 0 \\ 0 \\ 1 \\ 0 \end{pmatrix}, \quad v(2, \mathbf{0}) = \begin{pmatrix} 0 \\ 0 \\ 0 \\ 1 \end{pmatrix}. \quad (26)$$

The general solution of Eq. (17) is

$$\psi(x) = \int \frac{d^3 \mathbf{p}}{(2\pi)^3} N(\mathbf{p}) \sum_{\xi} [b(\xi, \mathbf{p}) u(\xi, \mathbf{p}) e^{ip \cdot x} + d^{\dagger}(\xi, \mathbf{p}) v(\xi, \mathbf{p}) e^{-ip \cdot x}] \quad (27)$$

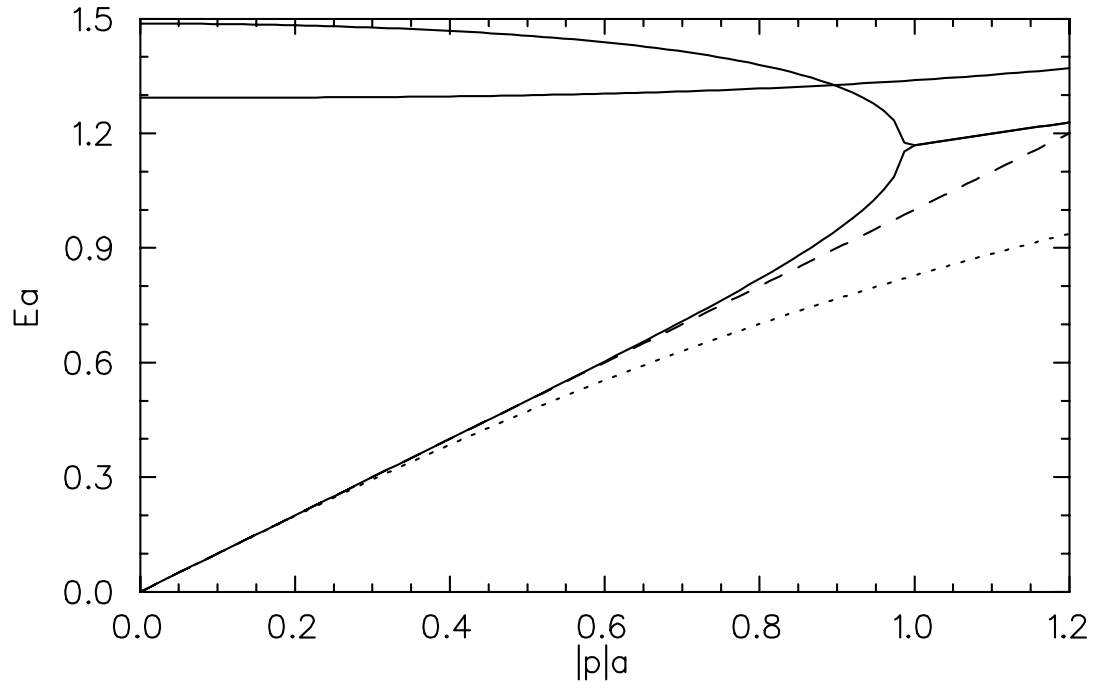


FIG. 1. The energy-momentum relation for a massless, free fermion from the improved action with 3-momentum  $\mathbf{p}$  in the (1,1,0) direction. Only the real parts of complex solutions are shown. The dashed(dotted) curve is the continuum(Wilson) result.

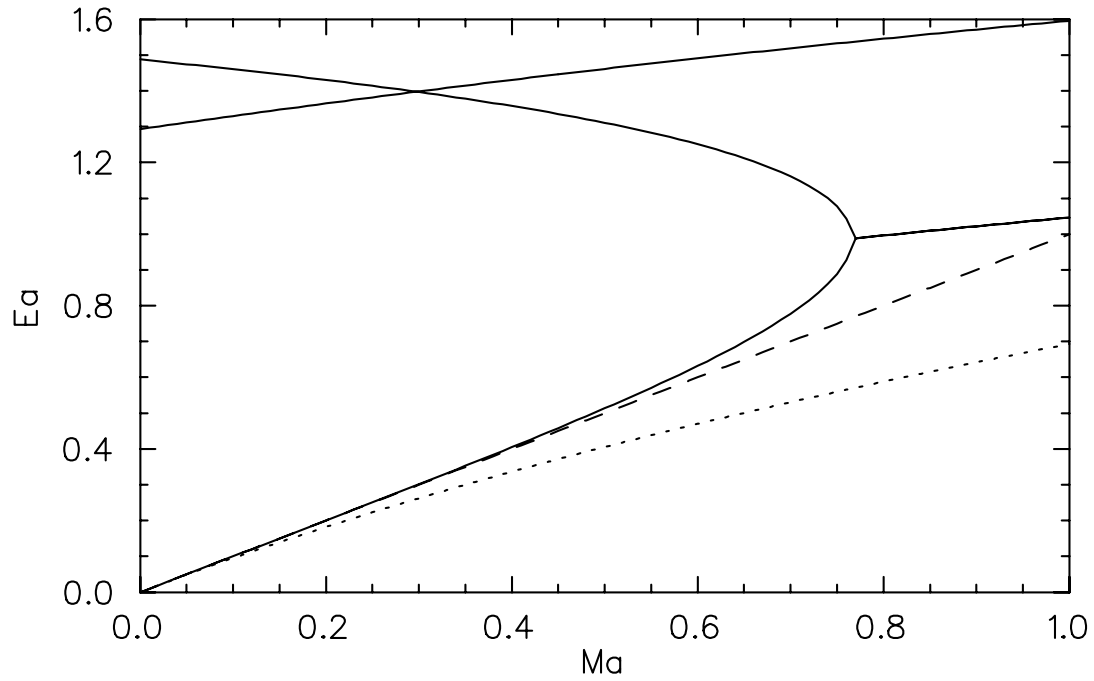


FIG. 2. The energy-mass relation for a stationary, free fermion from the improved action. Only the real parts of complex solutions are shown. The dashed(dotted) curve is the continuum(Wilson) result.

where  $b(\xi, \mathbf{p})$  annihilates a quark and  $d^\dagger(\xi, \mathbf{p})$  creates an antiquark. The normalization factor  $N(\mathbf{p})$  can be determined, for example, from the normalization of the quark propagator. By choosing the creation and annihilation operators to be normalized in the following way,

$$\{b(\xi', \mathbf{p}'), b^\dagger(\xi, \mathbf{p})\} = \{d(\xi', \mathbf{p}'), d^\dagger(\xi, \mathbf{p})\} = (2\pi)^3 \delta^3(\mathbf{p}' - \mathbf{p}) \delta^{\xi\xi'}, \quad (28)$$

the normalization factor is found to be

$$N(\mathbf{p}) = \left[ \frac{9L(p)}{(4\cosh Ea - \cosh 2Ea) \sinh Ea (4 - \cosh Ea) + 6 (2\sinh Ea - \sinh 2Ea) L(p)} \right]^{1/2}. \quad (29)$$

## B. $f_V$ and $Z_V$

The vector meson decay amplitude and the insertion of a vector current between hadron states can now be calculated at the classical level using the matrix elements

$$\langle 0 | V_\mu | q(\xi, \mathbf{p}) \bar{q}(\xi', \mathbf{p}') \rangle \quad \text{and} \quad \langle q(\xi', \mathbf{p}') | V_\mu | q(\xi, \mathbf{p}) \rangle$$

respectively. In each case, kinematics are chosen that corresponds to the numerical simulations of Sec. IV, which means that the decay amplitude is studied in the rest frame ( $\mathbf{p}' = -\mathbf{p}$ ), whereas the vector current insertion has no 4-momentum transfer ( $p' = p$ ). A consequence of these choices is that only  $\mu = 1, 2, 3$  are nonzero for the decay amplitude, and only  $\mu = 4$  is nonzero for the vector current insertion.

Using  $V_\mu^C$  as the vector current, the decay amplitude is

$$\begin{aligned} & \langle 0 | V_j^C | q(\xi, \mathbf{p}) \bar{q}(\xi', -\mathbf{p}) \rangle \\ &= N^2(\mathbf{p}) \bar{v}(\xi', -\mathbf{p}) \left[ -\frac{4i}{3} \sin p_j a + \frac{4}{3} \gamma_j \cos p_j a + \frac{2i}{3} \sin 2p_j a - \frac{1}{3} \gamma_j \cos 2p_j a \right] u(\xi, \mathbf{p}) \end{aligned} \quad (30)$$

$$= N^2(\mathbf{p}) \left[ \frac{4}{3} \cos p_j a - \frac{1}{3} \cos 2p_j a \right] \bar{v}(\xi, \mathbf{0}) \gamma_j u(\xi, \mathbf{0}) \quad (31)$$

$$= \bar{v}(\xi, \mathbf{0}) \gamma_j u(\xi, \mathbf{0}) \left[ 1 + \mathcal{O}(a^3) \right] \quad (32)$$

where Eq. (21) has been used. A similar derivation shows that Eq. (32) also holds for the local vector current,  $V_j^L$ , so the decay amplitude is classically improved up to  $\mathcal{O}(a^2)$  for both vector currents.

The expression for the current insertion is

$$\begin{aligned} & \langle q(\xi', \mathbf{p}') | V_4^C | q(\xi, \mathbf{p}) \rangle \\ &= N^2(\mathbf{p}) \bar{u}(\xi', \mathbf{p}') \left[ \frac{4}{3} \sin Ea + \frac{4}{3} \gamma_4 \cos Ea - \frac{2}{3} \sin 2Ea - \frac{1}{3} \gamma_4 \cos 2Ea \right] u(\xi, \mathbf{p}) \end{aligned} \quad (33)$$

$$= \delta^{\xi\xi'}. \quad (34)$$

Notice that there are no finite- $a$  errors here as required by current conservation. For the local current, it is found that



TABLE I. Simulation parameters.  $N_U$  is the number of gauge field configurations,  $a_{st}$  is the lattice spacing derived from the string tension,  $\kappa_c$  is the hopping parameter at the critical point and  $\kappa_s$  is the hopping parameter corresponding to the strange quark mass (from  $m_{K^*}/m_K$ ). The error in the last digit is bracketed.

Lattice	$N_U$	$\beta$	$a_{st}[\text{fm}]$	$\kappa$	$\kappa_c$	$\kappa_s$
Improved Action						
$6^3 \times 12$	200	6.25	0.4	0.162, 0.168, 0.174	0.1803(2)	0.1658(8)
$8^3 \times 14$	100	6.8	0.27	0.150, 0.154, 0.158	0.1638(2)	0.1561(5)
Wilson Action						
$6^3 \times 12$	200	4.5	0.4	0.189, 0.201, 0.213	0.2189(2)	0.2050(3)
$8^3 \times 14$	100	5.5	0.27	0.164, 0.172, 0.180	0.1857(3)	0.1779(7)

$$\langle q(\xi', \mathbf{p}) | V_4^L | q(\xi, \mathbf{p}) \rangle = \delta^{\xi\xi'} [1 + \mathcal{O}(a^3)] \quad (35)$$

which again displays the desired classical improvement.

Thus, although we are using an *unimproved* conserved current, the particular calculations being considered in this work are still improved to the level of the action. This conclusion will be valid for the numerical simulations as well, provided we create the external hadron states using operators that maintain the improvement. Local interpolating fields, such as those of Eqs. (8-10) which will be used in the present work, guarantee that classical improvement is not destroyed.

#### IV. NUMERICAL SIMULATIONS

Calculations were performed at two values of  $\beta$  with the improved action, corresponding to lattice spacings of 0.4fm and 0.27fm as derived from the string tension. For comparison, the Wilson action was also used to calculate at the same lattice spacings. Some details of the simulations are provided in Table I.

In all cases, we used pseudo-heatbath updating with periodic boundary conditions for the gauge fields. The lattices were thermalized with 4000 sweeps, and then 250 sweeps (200 sweeps) were discarded between each pair of improved (Wilson) configurations that was kept. A stabilized biconjugate gradient algorithm was used for the fermion matrix inversion. To maximize the number of useful time slices, Dirichlet boundary conditions were used for fermions in the time direction, with periodic boundary conditions in all spacial directions. The source was placed two timesteps away from the time boundary in every case, and for the 3-point correlators of  $R_P$ ,  $R_V$  and  $R_B$  we attached the vector current insertion to the lattice's centre time slice.

Fig. 3 shows the effective mass plot for a pseudoscalar meson with the improved action. The non-monotonic behaviour near the source ( $t = 3$  in Fig. 3) is a consequence of next-nearest-neighbour interactions, as discussed by Lüscher and Weisz [13]. The effect of these high-energy oscillations decreases as  $\kappa$  increases, and Fig. 3 shows that there is already an identifiable plateau at our smallest value of  $\kappa$ .

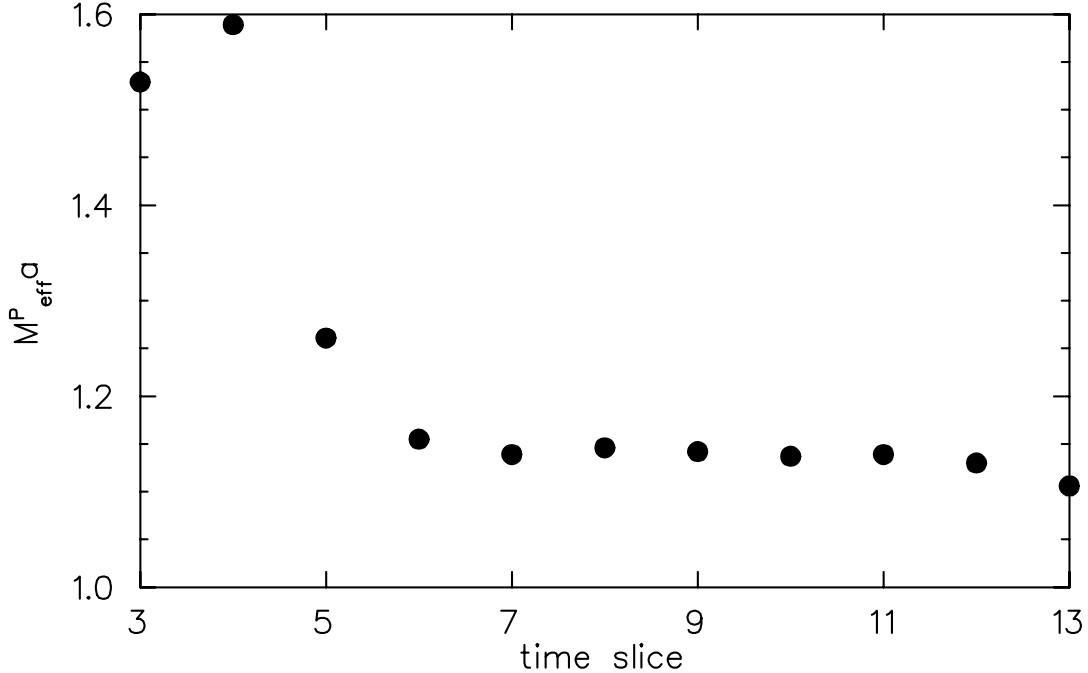


FIG. 3. The effective mass plot for a pseudoscalar meson using the improved action at  $\beta = 6.8$  with  $\kappa = 0.150$ .

To extract the mass from an effective mass plot such as Fig. 3, or to obtain  $Z_V$  or  $1/f_V$  from the appropriate plot, we require that the plateau contains at least three neighbouring points, and we never use the two time slices near the boundary (12 and 13 in Fig. 3) which can be affected by the Dirichlet boundary condition. The systematic uncertainties associated with choosing a plateau region will not be presented since we do not expect these uncertainties to affect the principal conclusions of our study. All statistical errors will be computed using half the distance between the 16th and 84th percentiles from 500 bootstrap samples.

The results for the renormalization factor, obtained from the improved action at  $\beta = 6.8$ , are shown for degenerate-mass quarks in Fig. 4. The value of  $Z_V$  that comes from using meson decay amplitudes ( $R_D$ ) in Eq. (5) is significantly smaller than the values that come from inserting a vector current between pion,  $\rho$  meson or nucleon states ( $R_P$ ,  $R_V$ ,  $R_B$ ), and this difference is a reflection of the finite- $a$  errors that are present in Eq. (5). To decide whether these finite- $a$  errors should be considered as large or small, a comparison is made to results from the Wilson action. Fig. 4 shows that the improved action results agree remarkably well with Wilson data at  $\beta = 6.0$ , while being clearly distinguishable from Wilson data (for  $R_D$ ) at  $\beta = 5.85$ .

By defining an effective hopping parameter which averages over the two quark flavours in a meson or baryon,

$$\frac{1}{2\kappa_{\text{eff}}} = \frac{1}{2} \left( \frac{1}{2\kappa_1} + \frac{1}{2\kappa_2} \right), \quad (36)$$

we can plot all of our data, involving degenerate and nondegenerate quarks, together. Fig. 5

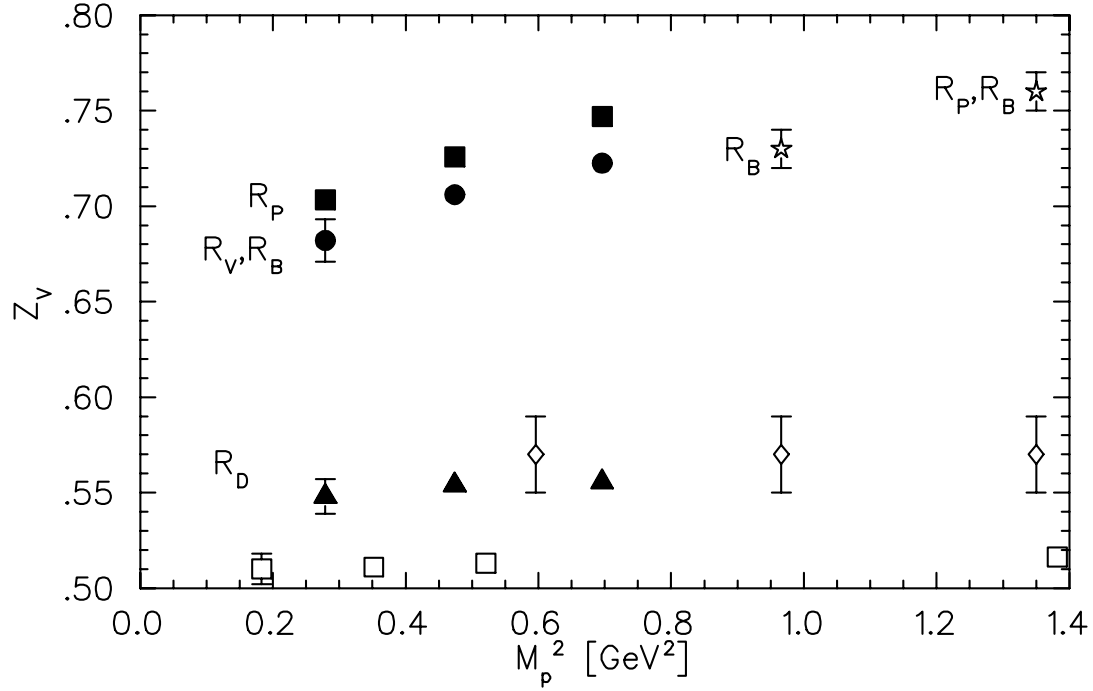


FIG. 4. The renormalization constant as a function of the pseudoscalar mass squared with degenerate quarks. Solid symbols are from the improved action at  $\beta = 6.8$ ; open stars [14] and diamonds [15] are Wilson at  $\beta = 6.0$ ; open squares [16] are Wilson at  $\beta = 5.85$ .

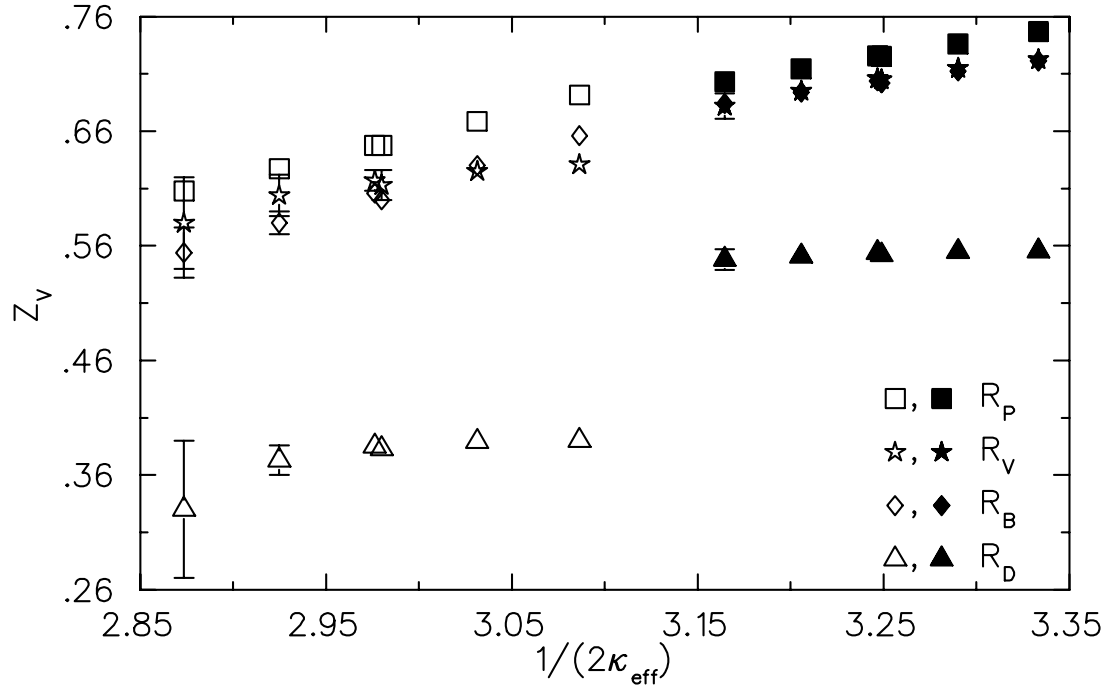


FIG. 5. The renormalization constant as a function of  $1/(2\kappa_{\text{eff}})$ . Open(solid) symbols are from the improved action at  $\beta = 6.25(6.8)$ .

shows that our improved action results for  $Z_V$  appear to be linear in  $1/(2\kappa_{\text{eff}})$ .

The chiral limit,  $\kappa = \kappa_c$ , is reached by extrapolating  $Z_V$ ,  $1/f_V$ , pseudoscalar meson masses *squared*, vector meson masses and baryon masses linearly in  $1/\kappa$ , using three data points (degenerate and nondegenerate quarks are used separately). In this way, we obtain the results of Fig. 6 for the renormalization factor without strange quark involvement. Also shown are the chiral limit values corresponding to the Wilson results of Fig. 4, and our own Wilson calculations at smaller  $\beta$ 's. Note that the improved action approximately resembles the trajectory of Wilson data, but translated horizontally to lattice spacings about three times as large. This is very similar to what was also found in a comparison of the mass spectra [7], and provides the first indication that the accuracy of calculations with tadpole-improved actions on coarse lattices persists beyond spectral quantities.

Fig. 7 shows the  $\rho$  meson decay constant without including the effect of  $Z_V$ , and with all Wilson quarks normalized by  $\sqrt{2\kappa}$ . Again, it is found that the improved action gives results which resemble the Wilson data, but at a lattice spacing about three times as large.

Our best determination of the  $\rho$  meson decay constant comes from the product of  $Z_V$  (obtained from  $R_D$ ) and  $1/(Z_V f_\rho)$ , which is shown in Fig. 8. The Wilson calculations can be divided into two categories: those which compute  $Z_V$  nonperturbatively as we have done in this work, and those which employ a perturbative estimate of  $Z_V$ , denoted by  $Z_{\text{pert}}$ . (The data in Fig. 8 with  $Z_{\text{pert}}$  use quarks which are *not* normalized by the naive  $\sqrt{2\kappa}$ , see the original papers for details.) The graph shows that both the improved and Wilson actions give nonperturbative results which are quite independent of lattice spacing over a large range of  $a$ , and which are near the experimental value. In contrast, the Wilson data using  $Z_{\text{pert}}$  approaches a similar continuum limit but with a noticeable dependence on  $a$ .

Having now discussed  $1/f_V$  in the chiral limit, let's return to our unextrapolated results, plotted in Fig. 9. Notice that the slope of our data is consistent with the observed slope from the two experimental points  $1/f_\rho$  and  $1/f_\phi$ , but as  $a \rightarrow 0$  the simulations appear to favour values larger than the experimental ones. We find it interesting that the UKQCD data, also shown in Fig. 9, displays the same tendency. In their paper [19], the UKQCD group concludes that this shift toward larger  $1/f_V$  values is the opposite of what would be expected from quenching, and they suggest that finite volume effects or lattice spacing effects may be responsible. The testing of such possibilities within the context of our  $\mathcal{O}(a^2)$  classically-improved, tadpole-improved action is much less computer-intensive than for the  $\beta = 6.2$  clover action, and might offer some valuable insight.

The hopping parameter corresponding to the strange quark as given in Table I, was determined from the experimental relation

$$\frac{m_{K^*}}{m_K} = 1.8 \tag{37}$$

by linear interpolation in  $1/\kappa$  between the two neighbouring data points. Using this, Table II gives our results for the three light vector meson decay constants and compares them to predictions from other groups.

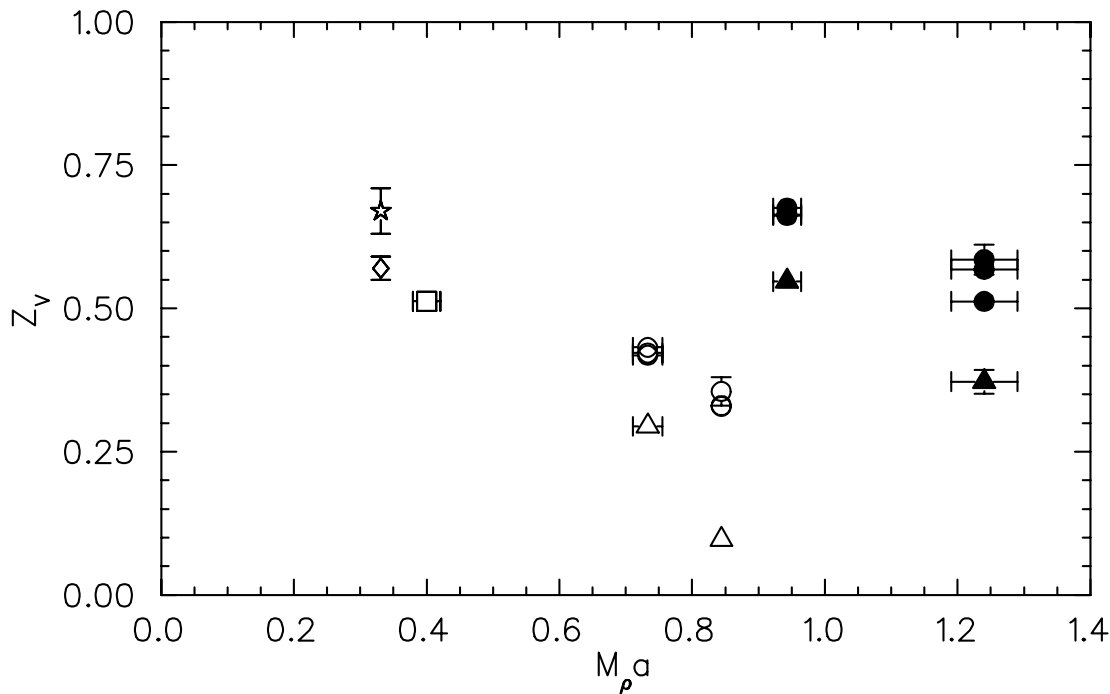


FIG. 6. The renormalization constant in the chiral limit. Solid(open) symbols are from the improved(Wilson) action. The open star, diamond and square are from Refs. [14], [15] and [16] respectively. The lowest-lying point at each  $M_\rho a$  is from the decay amplitude,  $R_D$ .

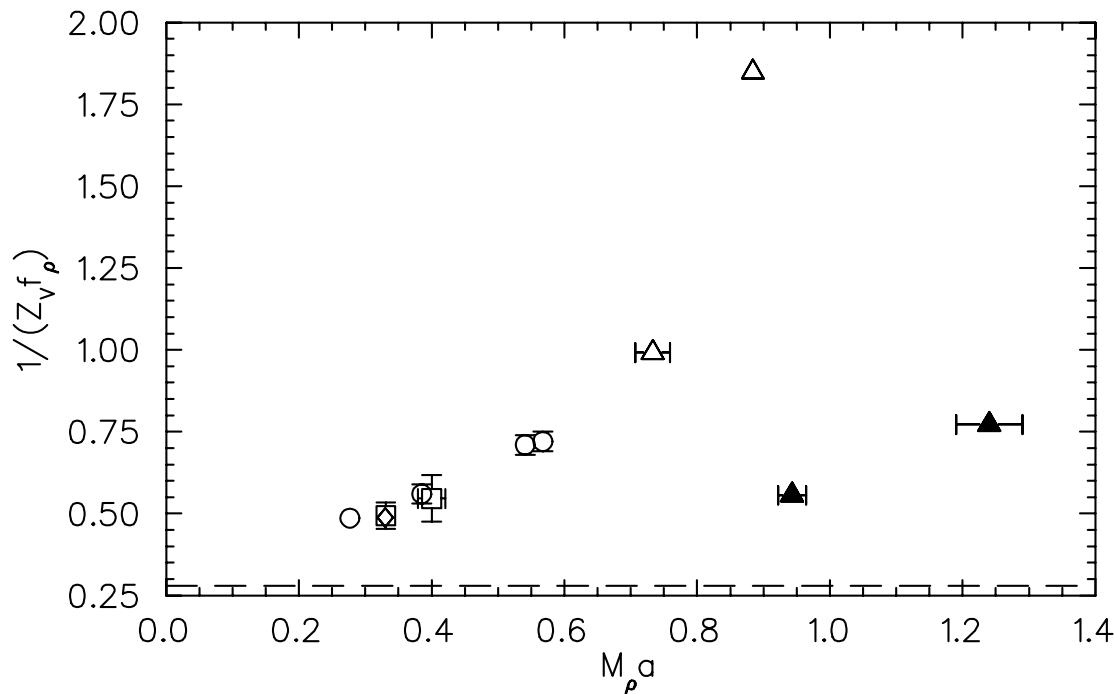


FIG. 7. The lattice decay constant in the chiral limit. Solid(open) symbols are from the improved(Wilson) action and the dashed line is the experimental value. Open squares, circles and diamonds are from Refs. [16], [17] and [18] respectively. All Wilson quarks are normalized by  $\sqrt{2\kappa}$ .

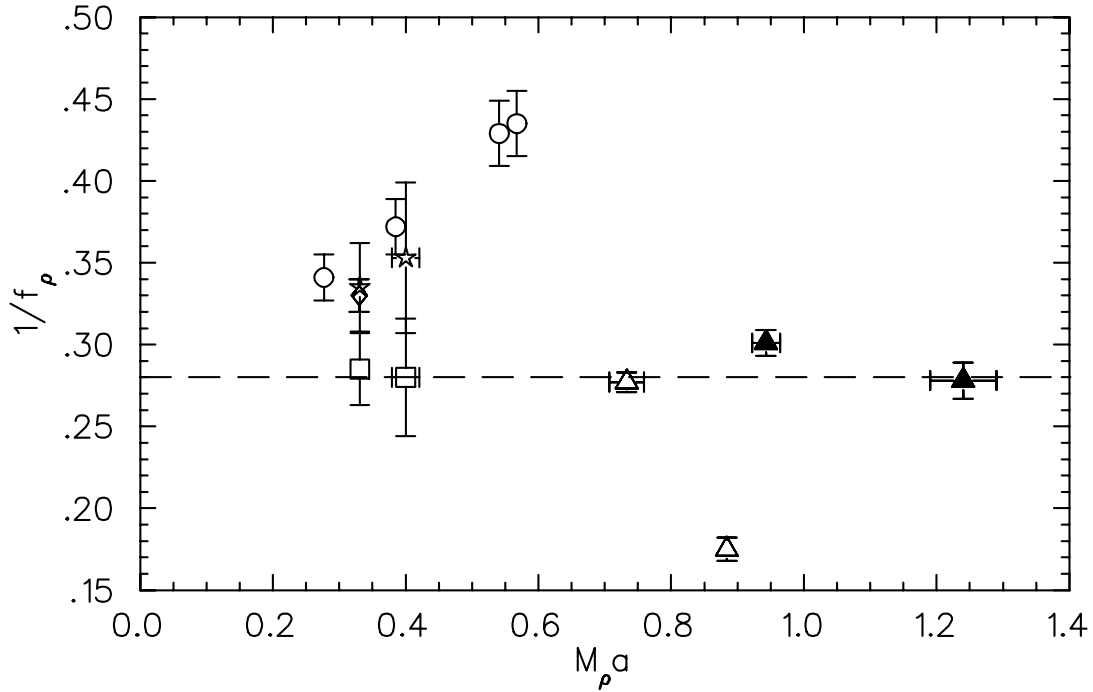


FIG. 8. The renormalized decay constant in the chiral limit. All symbols are defined as in Fig. 7. Squares and triangles use a nonperturbative determination of  $Z_V$ ; all other data rely on a perturbative estimate.

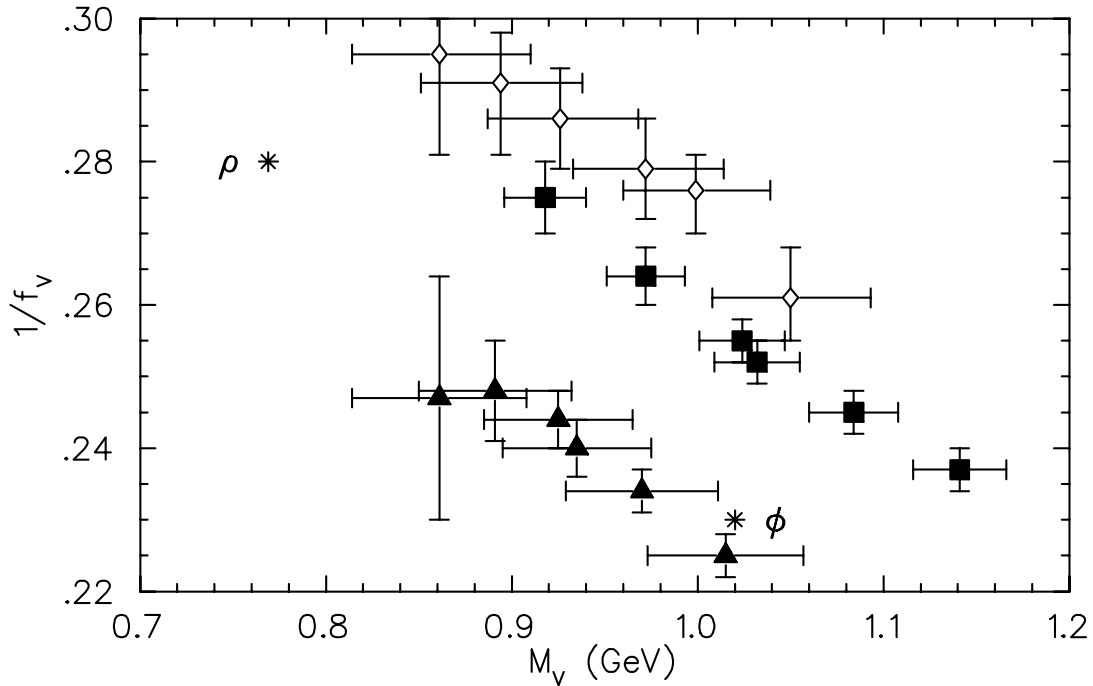


FIG. 9. Decay constant data before extrapolation/interpolation. Solid triangles(squares) are improved action data at  $\beta = 6.25$  (6.8), open diamonds are  $\beta = 6.2$  clover data [19], and the asterisks represent experimental data. The horizontal scale is set by the physical  $\rho$  meson mass.

TABLE II. The decay constants from various simulations. Only the largest  $\beta$  results from each reference are shown here. All clover and Wilson data use the perturbative renormalization constant  $Z_{pert}$ .  $a_\rho$  is the lattice spacing derived from the  $\rho$  mass.

Action	$a_\rho$ [fm]	$1/f_\rho$	$1/f_{K^*}$	$1/f_\phi$
improved, $\beta = 6.25$	0.32(1)	0.278(11)	0.255(6)	0.236(2)
improved, $\beta = 6.8$	0.242(5)	0.301(8)	0.284(5)	0.265(3)
Wilson, $\beta = 6.0$ , Ref. [18]	0.0845(1)	0.33(1)	—	—
Wilson, $\beta = 6.17$ , Ref. [17]	0.071(1)	0.34(1)	—	0.38(1)
clover, $\beta = 6.2$ , Ref. [19]	0.073(3)	$0.316^{+7}_{-13}$	$0.298^{+5}_{-9}$	$0.280^{+3}_{-6}$
Wilson, $\beta = 6.4$ , Ref. [20]	?	0.32(2)	0.32(1)	—
clover, $\beta = 6.4$ , Ref. [20]	?	0.25(2)	0.24(1)	—
experiment	—	0.28	—	0.23

## V. CONCLUSIONS

In this paper we have calculated vector current matrix elements and the renormalization factor in the light quark sector for an improved action on lattices with spacings of about 0.3 to 0.4fm. This is the first step in going beyond the mass spectrum with improved actions on coarse lattices.

The action used here is particularly simple. It has next-nearest-neighbour couplings to remove  $\mathcal{O}(a)$  and  $\mathcal{O}(a^2)$  errors at the classical level and also incorporates tadpole improvement. No special tuning of parameters and no field transformations are required with this action.

Vector meson decay constants and the vector current renormalization factor calculated with the improved action were found to be comparable to those with the Wilson action on lattices with about 1/3 the spacing. This is the same as the improvement found previously in mass calculations and it represents a very substantial saving in computer resources.

## ACKNOWLEDGMENTS

The authors are grateful to Peter Lepage for a helpful discussion. This work was supported in part by the Natural Sciences and Engineering Research Council of Canada.

## REFERENCES

- [1] F. Niedermayer, hep-lat/9608097, to appear in the proceedings of the 14th International Symposium on Lattice Field Theory, St. Louis, U.S.A., 1996.
- [2] R. Lewis and R. M. Woloshyn, hep-lat/9607059, to appear in the proceedings of the 14th International Symposium on Lattice Field Theory, St. Louis, U.S.A., 1996.
- [3] G. Heatlie, C. T. Sachrajda, G. Martinelli, C. Pittori, and G. C. Rossi, Nucl. Phys. B **352**, 266 (1992).
- [4] M. Lüscher and P. Weisz, Comm. Math. Phys. **97**, 59 (1985).
- [5] H. Hamber and C. M. Wu, Phys. Lett. B **133**, 351 (1983); W. Wetzel, Phys. Lett. B **136**, 407 (1984); T. Eguchi and N. Kawamoto, Nucl. Phys. B **237**, 609 (1984).
- [6] G. P. Lepage and P. B. Mackenzie, Phys. Rev. D **48**, 2250 (1993).
- [7] H. R. Fiebig and R. M. Woloshyn, Phys. Lett. B (in press).
- [8] K. G. Wilson, in *New Phenomena in Subnuclear Physics*, (Erice, 1975), ed. A. Zichichi, Plenum Press, 1977.
- [9] F. X. Lee and D. B. Leinweber, hep-lat/9606005, to appear in the proceedings of PANIC '96, World Scientific.
- [10] A. Boriçi and Ph. de Forcrand, hep-lat/9608105, to appear in the proceedings of the 14th International Symposium on Lattice Field Theory, St. Louis, U.S.A., 1996.
- [11] Peter Lepage, private communication.
- [12] A. X. El-Khadra, A. S. Kronfeld and P. B. Mackenzie, Report No. FERMILAB-Pub-96-074-T, hep-lat/9604004 (unpublished).
- [13] M. Lüscher and P. Weisz, Nucl. Phys. B **240**, 349 (1984).
- [14] G. Martinelli and C. T. Sachrajda, Nucl. Phys. B **316**, 355 (1989).
- [15] L. Maiani and G. Martinelli, Phys. Lett. B **178**, 265 (1986).
- [16] QCDPAX Collaboration, Y. Iwasaki *et. al.*, Phys. Rev. D **53**, 6443 (1996).
- [17] F. Butler, H. Chen, J. Sexton, A. Vaccarino and D. Weingarten, Nucl. Phys. B **421**, 217 (1994).
- [18] T. Bhattacharya and R. Gupta, Phys. Rev. D **54**, 1155 (1996).
- [19] UKQCD Collaboration, C. R. Allton *et. al.*, Phys. Rev. D **49**, 474 (1994).
- [20] C. R. Allton, V. Giménez, L. Giusti, F. Rapuano, hep-lat/9609017, to appear in the proceedings of the 14th International Symposium on Lattice Field Theory, St. Louis, U.S.A., 1996.